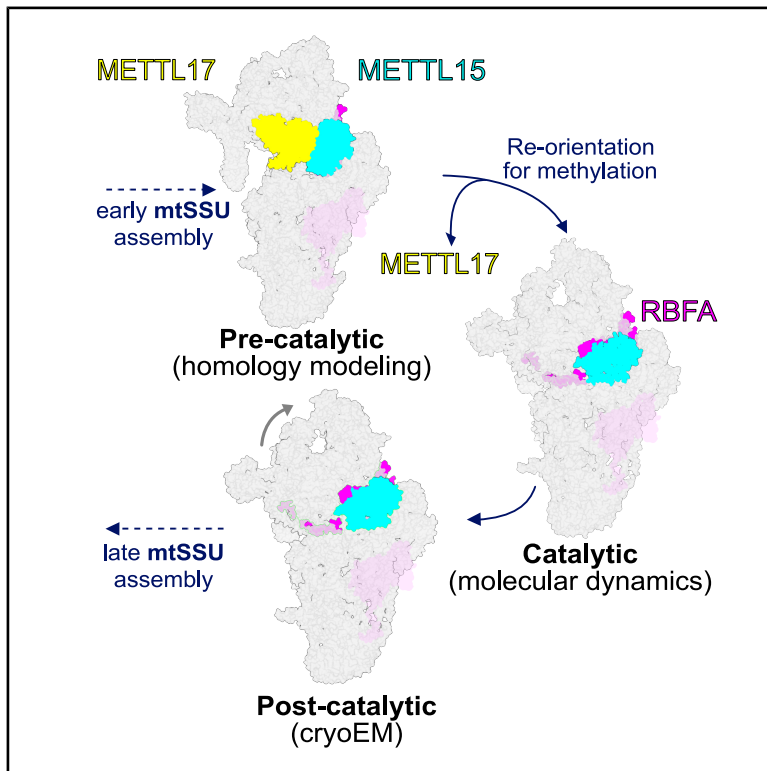


Structure

Mettl15-Mettl17 modulates the transition from early to late pre-mitoribosome

Graphical abstract



Authors

Yury Zgadzay, Claudio Mirabello, George Wanes, ..., Paul C. Whitford, Ondřej Gahura, Alexey Amunts

Correspondence

gahura@paru.cas.cz (O.G.), alexey.amunts@gmail.com (A.A.)

In brief

Zgadzay et al. resolve how methyltransferases Mettl15 and Mettl17 orchestrate mitoribosomal small subunit assembly. Mettl17 scaffolds Mettl15 in early pre-ribosomes, and its departure permits Mettl15 to reconfigure and methylate rRNA. Molecular dynamics simulations show this transition requires low energy, explaining how these factors regulate biogenesis.

Highlights

- Integrated modeling reveals transient assembly states of pre-mitoribosome
- Mettl17 plays a structural role by recruiting Mettl15 to form a heterodimer
- Mettl17 release triggers Mettl15's conformational rotation for rRNA methylation
- Mettl15 rotation enables catalytic access to C1486 with minimal energy barrier

Article

Mettl15-Mettl17 modulates the transition from early to late pre-mitoribosome

Yury Zgadzay,¹ Claudio Mirabello,^{2,11} George Wanes,^{4,5,11} Tomáš Pánek,⁶ Prashant Chauhan,^{7,8} Björn Nystedt,³ Alena Zíková,^{7,8} Paul C. Whitford,^{4,5} Ondřej Gahura,^{8,*} and Alexey Amunts^{9,10,12,*}

¹Department of Integrative Structural Biology, Institute of Genetics and Molecular and Cellular Biology, University of Strasbourg, Illkirch, France

²Department of Physics, Chemistry and Biology, National Bioinformatics Infrastructure Sweden, Science for Life Laboratory, Linköping University, 581 83 Linköping, Sweden

³Department of Cell and Molecular Biology, National Bioinformatics Infrastructure Sweden, Science for Life Laboratory, Uppsala University, Husargatan 3, SE-752 37 Uppsala, Sweden

⁴Department of Physics, Northeastern University, Boston, MA 02115, USA

⁵Center for Theoretical Biological Physics, Northeastern University, Boston, MA 02115, USA

⁶Department of Zoology, Faculty of Science, Charles University, Prague, Czech Republic

⁷Faculty of Science, University of South Bohemia, 37005 České Budějovice, Czech Republic

⁸Institute of Parasitology, Biology Centre, Czech Academy of Sciences, 37005 České Budějovice, Czech Republic

⁹University of Münster, Schlossplatz 8, 48143 Münster, Germany

¹⁰Department of Structural Biochemistry, Max Planck Institute of Molecular Physiology, Otto-Hahn-Str. 11, 44227 Dortmund, Germany

¹¹These authors contributed equally

¹²Lead contact

*Correspondence: gahura@paru.cas.cz (O.G.), alexey.amunts@gmail.com (A.A.)

<https://doi.org/10.1016/j.str.2025.08.002>

SUMMARY

The biogenesis of the mitoribosomal small subunit involves a dynamic network of assembly factors. Conserved methyltransferases Mettl15 and Mettl17 act on the solvent-exposed surface of rRNA. Binding of Mettl17 is associated with the early assembly stage, whereas Mettl15 is involved in the late stage. Here, we integrate structural data from *Trypanosoma brucei* with mammalian homologs and molecular dynamics simulations. We reveal how the interplay of Mettl15 and Mettl17 in intermediate steps links the distinct stages of small subunit assembly. The analysis suggests a model wherein Mettl17 acts as a platform for Mettl15 recruitment. Subsequent release of Mettl17 allows a conformational change of Mettl15 for substrate recognition. Upon methylation, Mettl15 adopts a loosely bound state which leads to its replacement by initiation factors, concluding the assembly. Together, our results indicate that assembly factors Mettl15 and Mettl17 cooperate to regulate the biogenesis process.

INTRODUCTION

In mitochondria, messenger RNA (mRNA) translation and protein synthesis are performed by the mitoribosome in association with the regulatory complex LRPPRC-SLIRP¹ and the OXA1L insertase at the inner mitochondrial membrane.^{2,3} The mammalian mitoribosome consists of three mitochondria-encoded RNA molecules with 19 modified nucleotides and at least 82 nuclear-encoded proteins.^{4–6} The formation of this complex machinery involves progressive assembly through the recruitment of assembly factors that act primarily on the ribosomal RNA (rRNA), triggering its gradual folding and modification, while mitoribosomal protein modules are formed.^{7–9} This allows for productive maturation through defined states that ultimately leads to the catalytic mitoribosome.¹⁰ Perturbations in the assembly pathway can underlie association of mitoribosomal dysfunction with various diseases.^{11–14}

Structural studies on *Trypanosoma brucei* mitoribosomal complexes showed that it is a good model for understanding fundamental principles of mitoribosomal assembly because its native pre-mitoribosomal complexes are biochemically more stable and contain most of the assembly factors observed in mammals and other eukaryotes.^{15–19} For example, *T. brucei* mitoribosomal large subunit biogenesis involves at least seven assembly factors shared with humans, including GTPases GTPBP7, MTG1, pseudouridinease RPUSD4, and methyltransferase MRM. The structures of intermediates with these factors allowed for a better understanding of their roles in the mitoribosomal assembly pathway.^{17,18}

The mammalian mitoribosomal small subunit (mtSSU) is highly dynamic and contains 12S rRNA with nicotinamide adenine dinucleotide associated with an rRNA insertion, 30 mitoribosomal proteins, and two iron-sulfur (Fe-S) clusters.^{20–23} The structure is arranged into two main regions defined as the body and

Table 1. Newly identified features of the *T. brucei* pre-mtSSU

Protein	Previous name or chain ID	TriTrypDB ID (Uniprot ID)	Newly described feature(s)
mt-SAF38	chains UY, Ue	Tb927.5.1720 (Q57ZP1)	assembly factor newly identified in the complex
Mettl15	mt-SAF14	Tb927.8.3130 (Q57W60)	homolog of Mettl15 (RsmH in <i>E. coli</i>) cofactor SAM
Mettl17	mt-SAF1	Tb927.11.5060 (Q385R2)	homolog of Mettl17 cofactor SAM iron-sulfur cluster Fe ₄ S ₄
RbfA	mt-SAF18	Tb927.11.10600 (Q383L9)	homolog of RbfA
mt-SAF16	–	Tb927.11.3670 (Q386E5)	homologs of <i>Saccharomyces cerevisiae</i> Mam33 ³¹ (Uniprot ID P40513), human p32 (Q07021 ³²) and <i>Chlamydomonas reinhardtii</i> mtSSU protein mS105 ³³ (A0A2K3DAY3)
mt-SAF19	–	Tb927.7.7080 (Q57XS8)	
mt-SAF25	–	Tb927.10.1820 (N/A)	
mS53	–	Tb927.9.6510 (Q38ET1)	residues 63–84 modeled
mt-SAF5	–	Tb927.11.15850 (Q381K1)	residues 560–596 modeled
mt-SAF10	–	Tb927.11.2180 (Q386U1)	residues 4–6 modeled
mt-SAF11	–	Tb927.10.15650 (N/A)	residues 148–156 modeled
rRNA	–	–	several regions modeled or adjusted (see method details)
mt-SAF10	chains UB, UC, UD, UF, UI, UJ, UM, UN	Tb927.11.2180 (Q386U1)	ligand acetyl coenzyme A
mt-SAF22		Tb927.10.11820 (Q389F9)	
mt-SAF27		Tb927.8.6040 (Q57YK5)	

head. The latter binds LRPPRC-SLIRP, which regulates mRNA delivery to a dedicated channel during translation initiation and undergoes conformational changes to accompany the movement of mRNA during the translation cycle.^{4,5,24} In skeletal muscle, exercise training-induced signaling leads to enhanced mitoribosomal activity that can bypass LRPPRC-SLIRP.²⁵ The assembly path involves at least 11 factors that facilitate binding of mitoribosomal proteins and construct the solvent-exposed surface of the rRNA, including the mRNA channel and the decoding center at the interface between the body and head.⁹

Structural studies have revealed that stable assembly intermediates of the small subunit can be divided into “early”²⁶ and “late”²² stages, each relying on distinct methyltransferases, Mettl17 and Mettl15, respectively. Mettl17 is also an Fe-S binding protein that serves as a checkpoint for mitochondrial translation.²⁷ However, the transition from the early to late stage, including the interaction between Mettl15 and Mettl17, has never been observed. It is also not clear what drives the release of Mettl17, which promotes maturation, primarily due to limitations in experimental design.

Studying mitoribosomal assembly intermediates experimentally is challenging because interactions between assembly factors are often dynamic, and the transient states can undergo dissociation when isolated for structural analysis. In addition, adding tags to assembly factors for protein purification can interfere with native interactions, and knockout strains might exhibit non-productive off-path configurations of pre-mitoribosome, thus compromising the interpretation. However, the recent development of new computational tools for the analysis of protein-protein interactions^{28,29} enabled studies on large nucleoprotein complexes involved in gene expression and associated with transient modifying enzymes.^{23,24} Thus, *in silico* approaches can reveal direct interacting partners and

propose models of sequential assembly of macromolecular complexes.

Here, we used the cryo-EM map of *T. brucei* mtSSU assembly intermediate¹⁵ and structural models of human early²⁶ and late²² intermediates. Leveraging recent computational advancements, we performed AlphaFold³⁰ analysis and molecular dynamics simulations to generate *in silico* models for previously undescribed states. This approach enabled us to propose a sequential mechanism that explains the structural basis for Mettl15-Mettl17 function on the pre-mitoribosome. PyMol sessions are available for all states as a Resource ([supplemental information](#)).

RESULTS

Mapping unassigned regions in the pre-mitoribosome uncovers Mettl15-Mettl17 heterodimer

An mtSSU intermediate from *T. brucei* has been previously studied by cryo-EM, but several regions in the map remained unassigned.¹⁵ Using the data from recently published structures of mammalian pre-mitoribosomal intermediates,^{22,26} we analyzed the *T. brucei* maps and identified a number of previously undescribed structural elements summarized in [Table 1](#).

First, we detected homologs of RbfA and Mettl15 (previously referred to as mt-SAF18 and mt-SAF14, respectively; [Figure S1A](#)), both of which are associated with Mettl17 (mt-SAF1) ([Figure 1A](#)). RbfA is a KH-domain containing assembly factor ([Figure 1B](#)) that scaffolds decoding center rRNA elements, contacts the 3' end of rRNA, and occupies the mRNA channel during ribosomal assembly in bacteria and mitochondria.^{22,34–37} Mettl15 is a class I SAM-dependent N⁴-methylcytidine (m⁴C) methyltransferase of bacterial origin that modifies the mtSSU rRNA at position C1486 (human numbering).^{38–41} Mettl17, in contrast, is a putative methyltransferase with no specific target,^{42,43} and the disruption

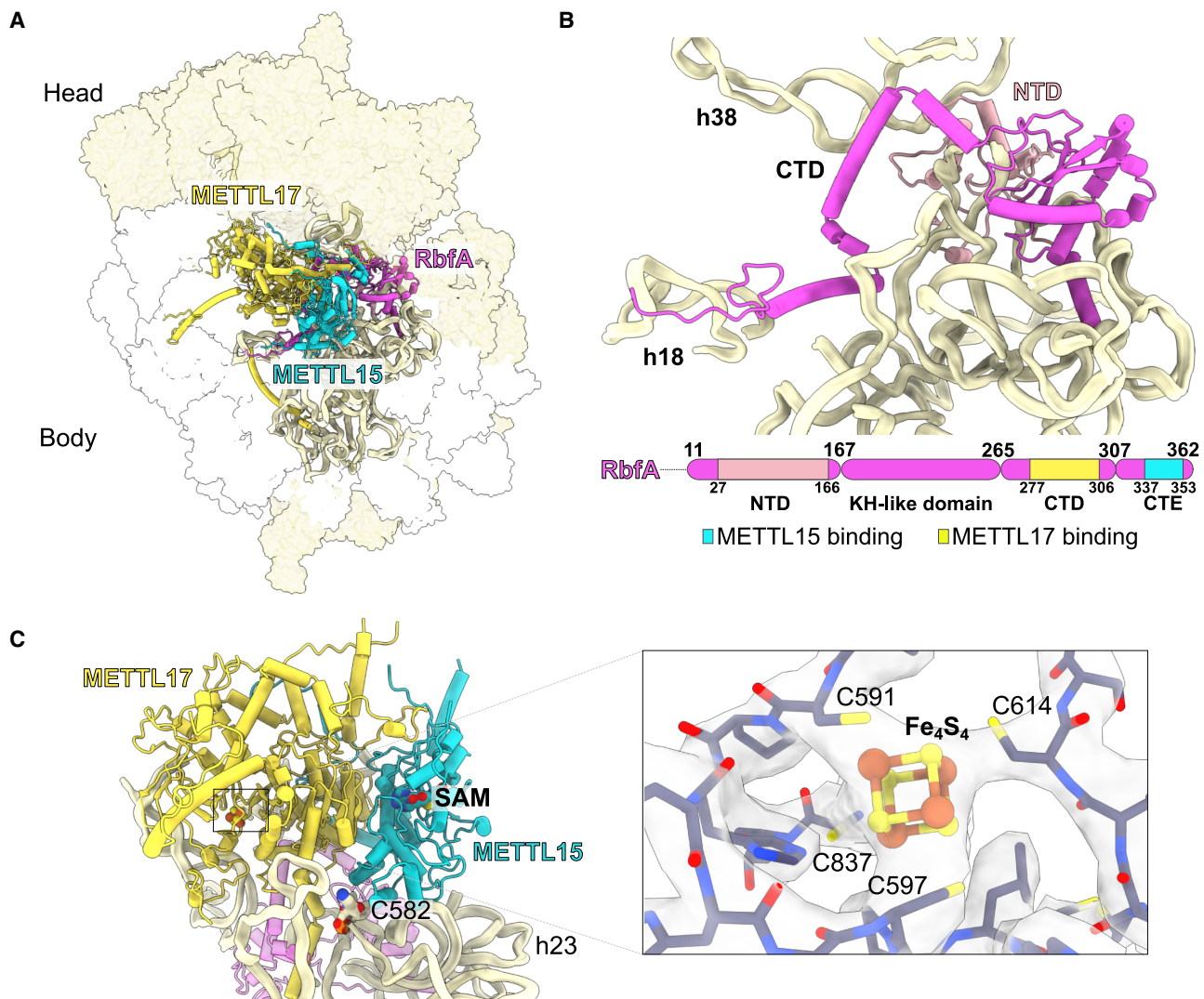


Figure 1. Dimer of Mettl15 and Mettl17 is found with RbfA in a *T. brucei* pre-mtSSU

(A) Structure of pre-mtSSU highlights Mettl15 (yellow), Mettl17 (cyan), RbfA (magenta), and rRNA (pale-yellow ribbon). Other assembly factors and mitoribosomal proteins are shown as white and yellow surfaces, respectively.

(B) Structure and schematic representation of RbfA and its interaction with rRNA. Mettl15, and Mettl17 interacting regions are indicated.

(C) Structure of the Mettl15-Mettl17 heterodimer with cofactors. A close-up view shows Fe_4S_4 with its coordinating residues.

See also [Figure S1](#) and [Table S1](#).

of its interaction with the pre-mitoribosome impairs other methyltransferases as well.^{38,39,41} Structurally, RbfA is anchored to the complex by its N-terminal extension, with the C-terminal domain binding Mettl17 and the C-terminal extension binding Mettl15. Together, these elements stabilize the subcomplex in a way that Mettl15 and Mettl17 form a heterodimer that is bound in the cleft between the head and body ([Figure 1C](#)). The Mettl15-Mettl17 heterodimer has the complexation significance score of 0.695, this score is defined as the maximal fraction of the total free energy of binding,⁴⁴ which indicates a specific interface, and the interaction surface area is 4,380 Å². In total there are 43 hydrogen bonds and ten salt bridges that stabilize the Mettl15-Mettl17 heterodimer ([Table S1](#)), which contribute to two main interfaces. The first interface comprises the N-terminal part of Mettl17 (residues 45–95) and C-terminal part of Mettl15 (residues 402–

470). The second interface involves catalytic domains of both Mettl17 and Mettl15 (residues 484–512 and 176–198, respectively). These data suggest that in *T. brucei* Mettl15 and Mettl17 form a complex.

Both methyltransferases in the structure contain a functional prosthetic group S-adenosyl methionine (SAM) ([Figure 1C](#)). In Mettl15, SAM is located 42 Å away from the methyltransferase target residue cytidine 582 (C582, equivalent of human C1486), implying a non-catalytic conformation. The Mettl15 conformation is different from that observed in the mammalian m⁴C1486-containing post-catalytic precursor,²² thus implying a pre-catalytic state. In Mettl17, there is a density corresponding to an iron-sulfur Fe_4S_4 cluster, consistent with the mammalian²⁶ and yeast²⁷ homologs. Thus, the previously proposed role of Mettl17 as an oxidative stress sensor and an Fe-S checkpoint

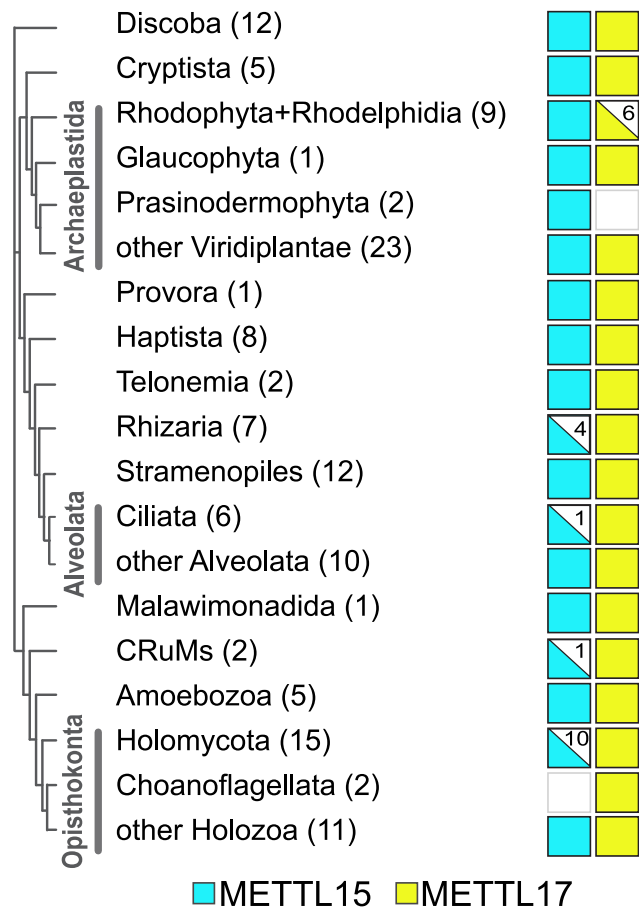


Figure 2. Mettl17 and Mettl15 are widely distributed across eukaryotes

Distribution in major eukaryotic groups mapped onto a phylogenetic tree.⁴⁷ The numbers in parentheses indicate the number of organisms searched in the respective group. Filled symbols represent presence in all organisms, half-filled symbols indicate presence in a subset of organisms, and empty symbols indicate absence. See also [Table S2](#) and [Data S1, S2, S3, and S4](#).

for mitochondrial translation^{27,45} may be conserved in a broad range of eukaryotes.

In addition, we assigned an uninterpreted region of density to trypanosomal assembly factor mt-SAF38¹⁹ ([Figure S1A](#)). Its overall fold is similar to a thioesterase, expanding a list of enzyme homologs identified in mitoribosomal subunits or their precursors.⁴⁶ Finally, we identified 13 hammerhead-shaped densities ranging from 17 to 22 Å in length, coordinated by tryptophan residues within a helix-loop-helix motif of pentatricopeptide repeat (PPR) proteins, which likely represent cofactors such as acetyl coenzyme A (acetyl-CoA) ([Figure S1B](#)).

Evolutionary conservation of Mettl17 suggests its role in recruiting Mettl15

To determine whether the Mettl15-Mettl17 heterodimer is a group-specific feature or may be widespread, we searched for these two methyltransferases in genomes of diverse eukaryotic organisms, followed by phylogenetic analysis. The search identified Mettl17 in 126 out of 134 organisms covering all major eukaryotic lineages. The cysteine residues coordinating the Fe₄S₄ cluster

in mammals and trypanosomes are conserved in most identified Mettl17 homologs. While Mettl15 is present in fewer organisms, it was identified in nearly all species where Mettl17 was present ([Figure 2](#), [Data S1, S2, S3, and S4](#)). This suggests that Mettl17 may be a prerequisite for the incorporation of Mettl15 into the pre-mitoribosome. Mettl17 is essential for mitochondrial translation in human cells,⁴³ for mitoribosomal assembly, translation, and viability in *T. brucei*,^{15,48} and for respiration in budding yeast,⁴⁹ but there is currently no evidence for the methyltransferase activity of this protein in any organism. Instead, human Mettl17 is required for methylation of rRNA by Mettl15.⁴³ Thus, consistently with other enzymes that adopted a structural role in the mitoribosome,⁵⁰ Mettl17 is an essential and conserved protein with no specific methylation target, whose primary function may be to facilitate Mettl15 integration into the pre-mitoribosome.

Mettl15 associates with Mettl17 on the pre-mitoribosome during early assembly stage

To clarify at which stage Mettl15 associates with Mettl17 on the pre-mitoribosome, we used structural models of human early²⁶ and late²² intermediates as references. The early and late intermediates contain Mettl17 and another methyltransferase, TFB1M (PDB ID 8CSP), whereas the late stage contains Mettl15 in a different conformation (PDB ID 7PNX). We generated AlphaFold²⁸ models of human Mettl17-TFB1M and Mettl15-TFB1M ([Figures 3A and 3B](#)). The two models obtained similar protein interface (ipTM) scores of 0.66 and 0.59, respectively, which would indicate reasonable confidence, according to the most recent benchmarking of AF prediction of multi-chain protein complexes.⁵² The AlphaFold model of Mettl17-TFB1M corresponds to the experimental dimer of the two proteins in the cryo-EM structure of the early state,²⁶ supporting the computational approach. We then used TFB1M as an anchoring point for superposition of Mettl15-TFB1M from the predicted model onto the early intermediate ([Figure 3C](#)). The superposition shows that Mettl15 is compatible with Mettl17, except minor clashes observed between a loop in Mettl17 (residues 220–247) and Mettl15 (residues 205–249). However, the Mettl17 loop has relatively high B-factor compared to rigid parts of the protein in current structures ([Figure S2](#)), indicating it is rather flexible and could attain alternative conformations when in complex with Mettl15. This suggests that Mettl15 could be structurally co-localized with Mettl17, TFB1M, and RbfA on the pre-mitoribosome. This is further supported by biochemical evidence, as TFB1M readily co-immunoprecipitates with Mettl15.³⁹ Thus, Mettl15 potentially associates with the pre-mitoribosome during the early assembly stage, possibly co-constituting a state with all three methyltransferases bound. To visualize protein-protein interactions of the three proteins on the mitoribosome, we used PDBePISA⁵¹ to calculate buried surface area between neighboring proteins. The visualization of the protein-protein network is shown in [Figure 3C](#), and specific protein parameters are given in [Table S1](#).

Pre-mitoribosome with Mettl15 and Mettl17 represents a pre-catalytic state

To establish the context of the pre-mitoribosome for the association of Mettl15 with Mettl17 and determine the state of the assembly, we constructed and refined a model of the human pre-mitoribosome with the Mettl15-Mettl17 heterodimer, using the

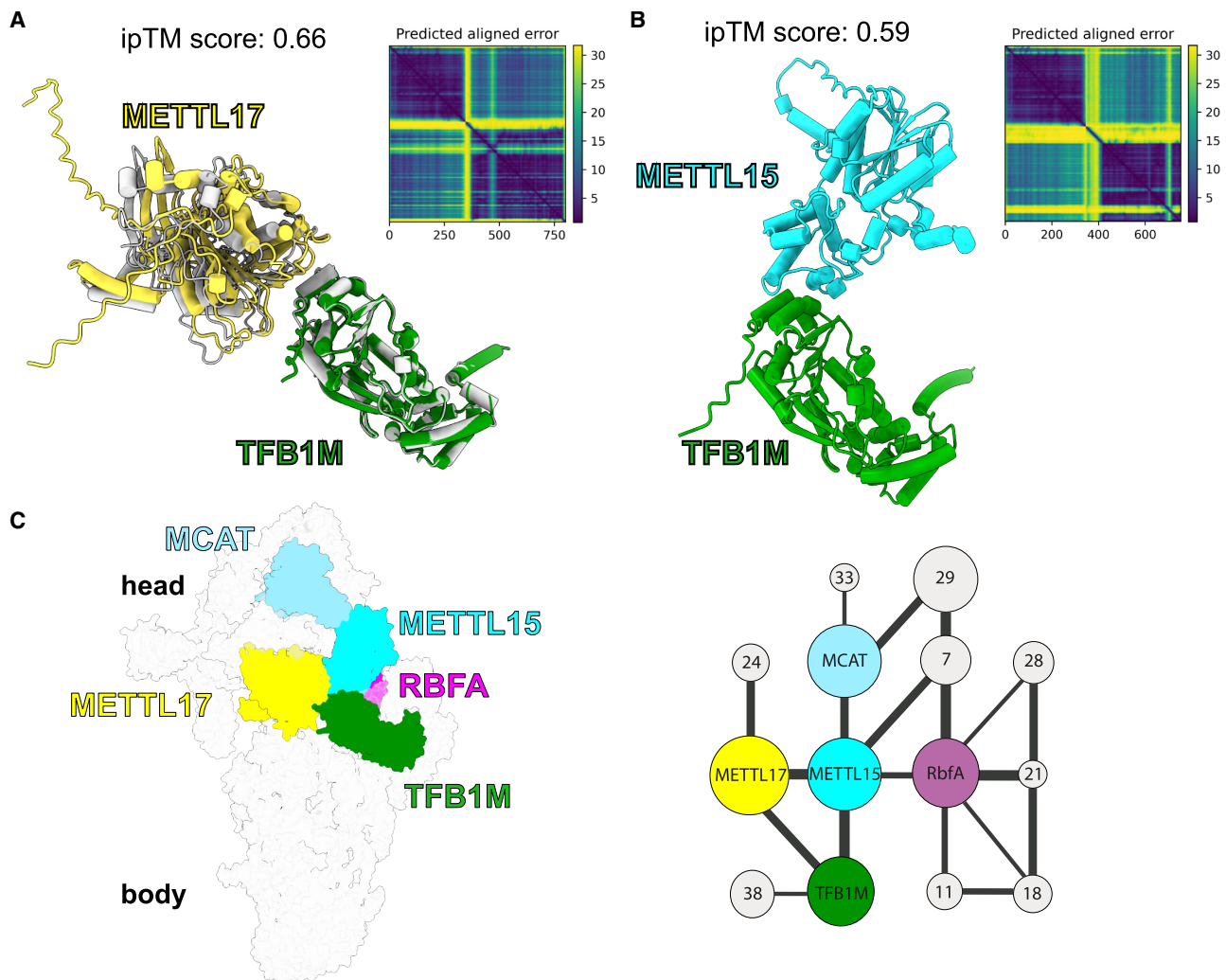


Figure 3. Modeling of early pre-mtSSU with Mettl15

(A) AlphaFold model of Mettl17-TFB1M superposed with the experimentally determined model of the early state (gray, PDB 8CSP).

(B) AlphaFold model of Mettl15-TFB1M.

(C) Left, model of early pre-mtSSU with all three methyltransferases, including Mettl15. Right, schematics of protein-protein interactions of methyltransferases, other assembly factors (colored nodes), and mitoribosomal proteins (gray nodes). The node size corresponds to relative molecular mass of protein subunits, and the connector width corresponds to the relative solvent accessible interface area buried between the subunits, calculated with PDBePISA v.1.52.⁵¹ For more details, see Table S1.

See also Figures S2 and S3; Table S1.

T. brucei structure as a template. We started the modeling by superposing human Mettl17 (PDB ID 8CST) and Mettl15 (PDB ID 7PNX) onto the *T. brucei* structure with the conserved rRNA core to obtain a model of the heterodimer. In the initial superposition, a short surface-exposed flexible insertion loop of human Mettl17 (residues 232–240) clashed with Mettl15 at the interface. It exhibits a variable length and sequence among homologs (Figure S2), suggesting it can adopt an alternative conformation compatible with dimer formation. The clash was fixed by relaxation with Amber.⁵³ Next, we aligned the Mettl15-Mettl17 model onto the early assembly stage structure of the human mitoribosome (PDB ID 8CST) using Mettl17 as an anchor (Figure S3). A knot between residues 304–312 of Mettl15 and residues of 1,076–1,081 of the rRNA was fixed by rebuilding

the protein loop with AlphaFold (see STAR Methods). Here, the position of Mettl15 is rotated by 45° compared to the post-catalytic state. The active site with the cofactor is located more than 40 Å from its target nucleotide C1486. The exact distance could not be calculated, because this rRNA region is disordered in the model. Since the position of Mettl15 is compatible with the human early-stage pre-mitoribosome, we conclude that the modeled intermediate with Mettl15-Mettl17 heterodimer corresponds to a pre-catalytic state (Figure S3).

Molecular dynamics simulations suggest how Mettl15 recognizes C1486

Since neither reported structures nor our models produced a catalytic state, where Mettl15 is bound to C1486, we used

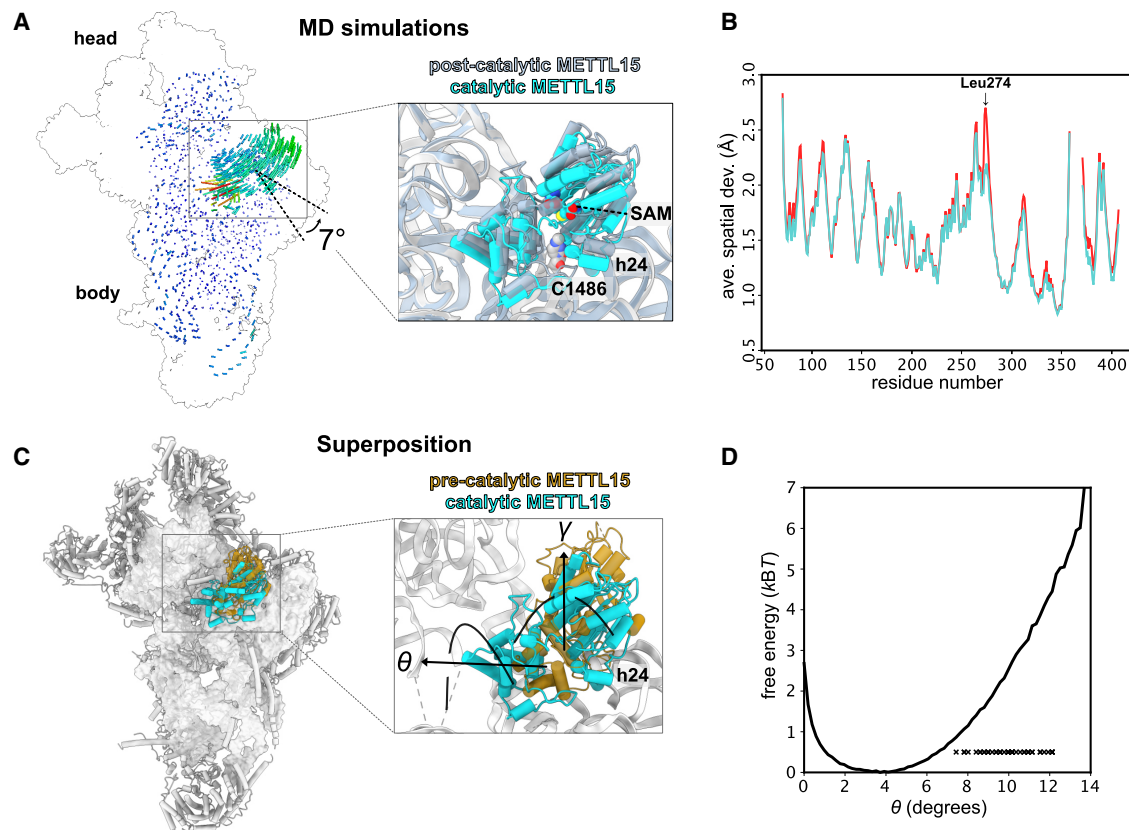


Figure 4. Simulation reveals low-energy structural fluctuations about post-catalytic configuration

(A) Comparison of Mettl15 orientations between catalytic (cyan) and post-catalytic (smoky blue) states based on superposition of the mtSSU. Shifts between equivalent Mettl15 C α atoms and rRNA phosphorus atoms in the different states are color-coded using the spectrum from dark blue to red, corresponding to the range from 0 to 20 Å.

(B) a.s.d of Mettl15 calculated with respect to the post-catalytic conformation. There are no major intramolecular structural deformations required to adopt orientations in which SAM is proximal to C1486 (restrained in red and unrestrained in cyan). The most notable difference is an increase of ~ 0.5 Å in Leu274.

(C) Comparison of Mettl15 orientations between pre-catalytic (brown) and catalytic (cyan) states. The angles describing Mettl15 rotation between the states are indicated.

(D) Free energy of Mettl15, calculated from a simulation without SAM-C1486 restraints (i.e., unrestrained). When the restraint is included, short distances between SAM and C1486 (<7 Å) can be reached when Mettl15 is rotated/tilted by $\sim 7^\circ$ - 12° . Each "x" indicates a simulated conformation in which the distance is small (<7 Å) in the restrained simulations. These domain orientations are associated with small increases in free energy, indicating that thermal energy is sufficient for Mettl15 to spontaneously adopt catalytically compatible poses.

See also Figure S4.

molecular dynamics simulations to gain insight into the motions that could allow Mettl15 to reach a catalytically compatible state. Specifically, we asked whether catalytically competent states are readily accessible from post-like configurations, or if a more substantial conformational change is required. To address this, we generated candidate structural models of a catalytically compatible state using a simulation-based molecular modeling strategy. In this approach, the distance between the Mettl15-bound SAM molecule and C1486 is restrained, while post-catalytic-specific interactions with the mtSSU are also preserved (defined based on the available post-catalytic state). For this purpose, we used an all-atom structure-based (SMOG⁵⁴) force field, where the post-catalytic structure (PDB ID 7PNX²²) is explicitly defined to be the global potential energy minimum. Structure-based force fields are well-suited to investigate low-energy structural fluctuations since they provide predictions of molecular flexibility that are consistent with experimental B-factors⁵⁵

and more detailed explicit-solvent simulations.⁵⁶ In addition, SMOG force fields have been applied extensively to characterize molecular flexibility and large-scale rearrangements in bacterial,⁵⁷ mitochondrial and cytosolic ribosomes.^{4,58}

Our simulations indicate that large-scale structural deformations in Mettl15 are not required for Mettl15-bound SAM and C1486 to juxtapose. To demonstrate the structural change required, we introduced a restraint between atom C41 of C1486 and the sulfur atom of the Mettl15-bound SAM molecule. In addition, we defined the rRNA residues proximal to C1483 to be disordered (i.e., residues U1477 to C1494 and A1555 to G1570; see STAR Methods), since they are unresolved or have large B-factors in the pre-catalytic state (PDB ID 8CST). We find that introducing the restraint leads to a visible rotation of Mettl15, relative to the post-catalytic state (Figure 4A), where C1486 and SAM are in close proximity (~ 6.5 Å). Rotation of Mettl15 is facilitated by small-scale bending motions around

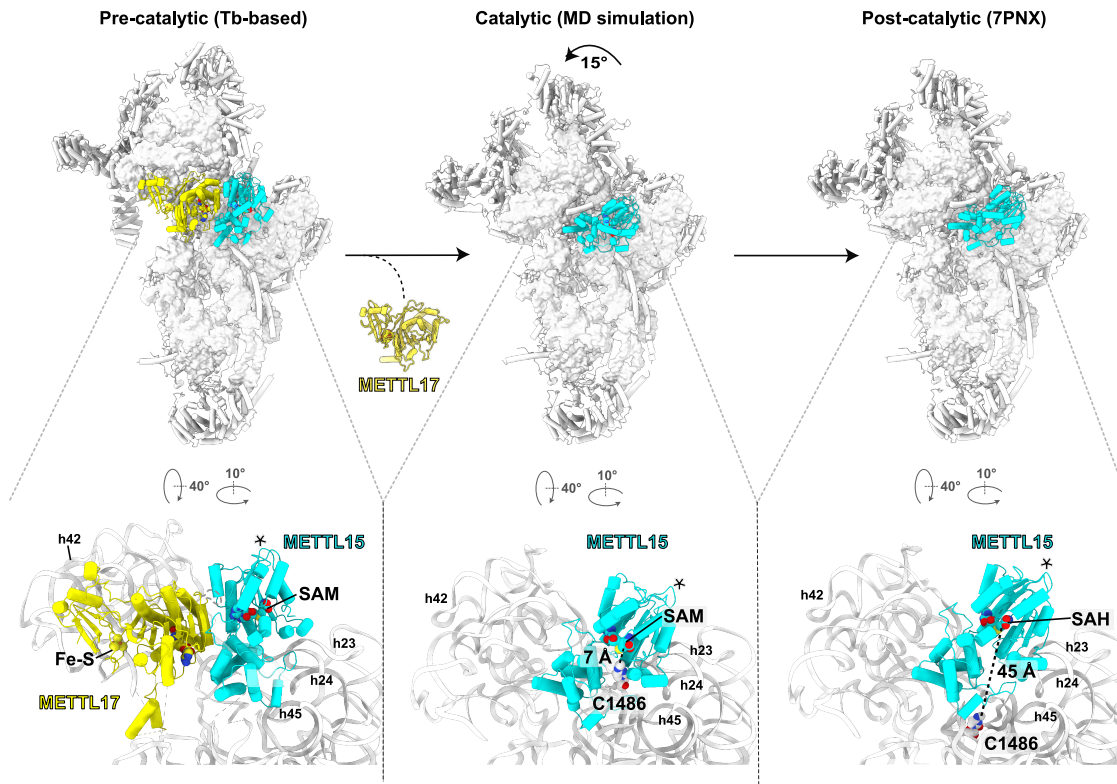


Figure 5. Sequential steps of assembly with Mett17 and Mett15

Left, *T. brucei* based model of human pre-mtSSU (PDB ID 8CST) with Mett17-Mett15. Middle, model from molecular dynamics simulations with rearranged Mett15 bringing it to the substrate for its methylation. Right, model of the post-catalytic state (PDB ID 7PNX), in which the target nucleotide C1486 is resolved. The estimated distances between the target nucleotide and Mett15 cofactor SAM are shown and selected rRNA helices are annotated in the close-up views. Asterisks indicate equivalent elements in the three states. See also [Video S1](#).

residues Lys271 to His279. To further characterize these deformations, we performed a second set of simulations in which the restraint was not included. We then compared the average spatial deviation of each residue in Mett15 after alignment to a post-catalytic structure ([Figure 4B](#)). The most significant difference between the restrained and unrestrained simulations was found for residue Leu274, where the average spatial deviation (a.s.d) value increased only slightly, from ~ 2.1 Å to ~ 2.7 Å.

To describe the rotational motion of Mett15, we calculated rotation (γ) and tilting (θ) angles ([Figure 4C](#); see [STAR Methods](#)). The rotation angle (γ) was defined as rotation that is parallel to that observed between the pre- and post-catalytic structures. In addition, the tilting angle (θ) is defined as any additional rotation that is orthogonal to γ . For reference, (γ, θ) are ($0^\circ, 0^\circ$) for the post-catalytic state and ($-45^\circ, 0^\circ$) for the pre-catalytic state. In simulations that included the C1486-SAM restraint, we calculated the rotation and tilt angle for all conformations in which the SAM-C1486 distance was less than 7 Å. Many of these conformations were associated with low rotation angles ($< 3^\circ$) and larger tilting angles (7° – 12°), calculated relative to the post-catalytic state.

After generating structural models for the mtSSU where Mett15 is in a catalytically compatible position, we asked whether these conformations are likely to be associated with large energetic penalties/barriers, or if thermal energy is sufficient for frequent fluctuations between post-like and catalytic conformations. To probe

the energetics of these tilted conformations, we used our unrestrained simulations to calculate the free energy as a function of tilt angle. This showed that tilt angles of 7° – 12° are only associated with an increase in free energy of ~ 1 – $5 k_B T$, relative to the post-catalytic structure ([Figure 4D](#)). While our model does not include specific interactions that stabilize the putative catalytic conformation, the low energy required for fluctuations from the post-catalytic conformation suggests that the associated free-energy barrier is likely to be relatively small (e.g., a few $k_B T$). This general scale of the barrier can be used to estimate the timescale for interconversion via the relation $\tau = C \exp(\Delta G/k_B T)$, where the exponential prefactor C can be estimated as roughly $1 \mu s$,⁵⁹ which would indicate that fluctuations between post-catalytic and catalytically competent conformations of Mett15 are likely to occur on timescales of ~ 10 – $100 \mu s$. This analysis provides an order-of-magnitude estimate of the timescale, where future calculations may employ more detailed models (e.g., all-atom explicit-solvent simulations) in order to dissect the precise interactions that control the kinetics of this rearrangement.

Sequential steps of small mitoribosomal subunit assembly involving Mett17 and Mett15

To establish the molecular sequence of Mett17 and Mett15 function on the pre-mitoribosome, we ordered the previously obtained structural insights into a series ([Figure 5](#); [Video S1](#)). First,

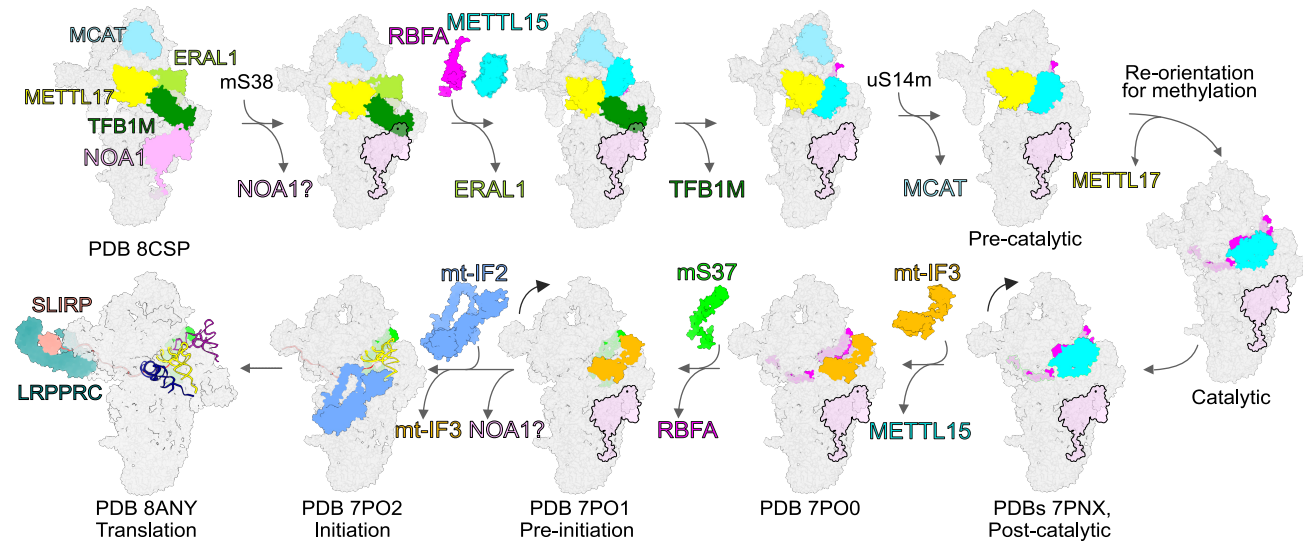


Figure 6. Proposed mtSSU pathway with precursors containing Mettl15-Mettl17 heterodimer and the pre-mtSSU with three methyltransferases

Assembly and initiation factors are shown as colored-coded surfaces. Mitoribosomal proteins and RNA are shown as gray surfaces. A recent study indicates that NOA1 (semitransparent), therein referred to as MTG3, remains associated with pre-mtSSU until the formation of the initiation complex in an alternative assembly pathway.⁶⁰ See also [Data S5](#).

the model from the early assembly stage with TFB1M, along with the *T. brucei*-based model of the Mettl15-Mettl17 heterodimer represents a pre-catalytic state. The next state obtained from molecular dynamics simulations, involves a rearrangement of Mettl15 with a 45° rotation, bringing SAM within 7 Å from the target to provide substrate for its methylation. Since RbfA, and not TFB1M, is present in the model, it is possible that the association of RbfA and the dissociation of TFB1M lead to a disruption of contacts between Mettl15 and Mettl17 resulting in the departure of Mettl17 from the pre-mtSSU. Therefore, only upon the release of Mettl17 can Mettl15 rotate toward C1486 to induce methylation. This sequence of events provides Mettl15 with the conformational space to approach its rRNA target site as predicted by the simulations (Figure 4). Finally, when methylation is accomplished, the conformation of Mettl15 changes again with a backward rotation to adopt a loosely bound state with SAM being 45 Å away from the target. This would ultimately lead to the replacement of Mettl15 by initiation factors in the late stage marking the completion of the mtSSU assembly as previously reported.²²

This architecture defines Mettl17 as the key factor that structurally orchestrates the series of assembly events. On one hand, its presence allows the binding of the methyltransferase Mettl15 required for rRNA maturation, and on the other hand, its departure provides the conformational potential of Mettl15 central domains that facilitates the rRNA maturation. Thus, Mettl17 stimulates the modification without exhibiting enzymatic activity.

DISCUSSION

In this analysis, we present an *in silico* model of human pre-mitoribosomal assembly, revealing that coupled methyltransferases Mettl15 and Mettl17 are involved in previously unde-

tested, transient assembly states (Figure 6). Our findings indicate that Mettl17 functions as a recruitment factor for Mettl15, forming a structural checkpoint for early assembly stages. This association suggests a broader quality control mechanism where Mettl17, alongside TFB1M, stabilizes Mettl15 and pauses maturation. Release of Mettl17 then facilitates Mettl15's conformational change on the pre-mitoribosome, allowing catalytic methylation of the rRNA, which aligns with observations of the folded rRNA region in this pre-mtSSU assembly.²² The precise mtSSU head position during C1486 methylation could differ, since it is rotated between pre- and post-catalytic state by 15°. Upon completion of methylation, Mettl15 is released, and the subunit core can move toward its functional conformation (Figure 6). A PyMol session with all the states is available as [Data S5](#). Our integrative structural analysis not only suggests a more complete picture of the mechanistic assembly process but also provides an experimentally testable hypothesis regarding a potential quality-control mechanism.

These steps of mitoribosomal assembly are particularly important in the context of biochemical, physiological, and behavioral observations in animals lacking Mettl15.⁶¹ In mice, the loss/ablation/downregulation of Mettl15 has been shown to lead to sub-optimal muscle performance, decreased learning capabilities, and lower blood glucose level after physical exercise.⁶² The same study, as well as results obtained earlier for cell cultures³⁹ also reported accumulation of the RbfA factor, and our model is consistent with these data.

SAM is essential for RNA processing in mouse embryonic fibroblasts and skeletal muscle.⁶³ Although Mettl17 retains the features typical of class I SAM-dependent methyltransferases,⁴² it does not methylate the 12S rRNA region, despite coming into contact with it during assembly. Our models suggesting that Mettl17 acts in recruitment of Mettl15 explain why loss of Mettl17

leads to around 70% reduction in the methylation, resulting in the impaired translation of mitochondrial protein-coding genes and consequent changes in the cellular metabolome.⁴³ Therefore, it appears that Mettl17 acts as an enhancer of mtSSU rRNA stability without being directly involved in RNA modification. Targeting of Mettl17 has recently been proposed as a therapeutic approach to suppress colorectal cancer xenograft growth, due to its importance for energy metabolism and maintenance of reactive oxygen species levels during ferroptotic stress.⁶³ Our findings rationalize the central mechanistic function of Mettl17 in the context of mitochondrial biogenesis. It also provides a more complete description of mtSSU assembly and proposes a plausible explanation for the sequential maturation of the human mitoribosome. Because the two methyltransferases, Mettl15 and Mettl17 co-exist in most eukaryotes, the described functional coupling most likely predates the last common eukaryotic ancestor, and its function presumably became vital as a consequence of the evolution of mitochondrial ribosomes during eukaryogenesis.

Finally, our methodology shows how integrating molecular dynamics with template-based modeling can reveal steps missed in experimental captures due to their transient nature. Although this study has limitations that require further experimental validation, the combined methodology presented here may serve as a more general complementary approach for revealing missing mechanistic steps of transient associations. Together with automated workflows for model building like CryFold⁶⁴ or ModelAngelo,⁶⁵ that further integrate AlphaFold-predicted structures,⁶⁶ scaled up by deep learning systems that generate protein ensembles,⁶⁷ this approach can be used for exploring dynamic properties of complex macromolecular systems where only partial experimental data are available. Our work underlines the importance of studying intricate biological processes in combination with advanced computational analyses in order to ultimately predict protein function and derive biogenesis pathways.

Limitations of the study

In this study, we integrate available structural data with model predictions and molecular dynamics simulations to explore previously undetected intermediate states of mtSSU assembly that have eluded experimental characterization. We identified two distinct states and described the features that determine dependence on the specific assembly factor Mettl17 (Figures 5 and 6, supplemental information). However, the resulting *in silico* models derived from our analysis require experimental validation. Additionally, we tested only a subset of available structures in this study, which constrained the starting points for our molecular dynamics simulations. As a result, some transitional states may not have been identified using this approach. Moreover, while we propose a plausible composition of the pre-mitoribosome at several stages and identify structural features that dictate the biogenesis pathway, the precise orientations of associated factors and the mtSSU head remain important areas for further investigation. Lastly, although we found that Mettl17 acts as a platform for Mettl15 recruitment and that its subsequent release enables a conformational change in Mettl15 for substrate recognition, understanding the energetic driving forces behind these events is an essential next step. Together, future mechanistic experiments in combination with comple-

mentary *in silico* approaches presented here and all-atom simulations are expected to offer a foundation for elucidating how complex networks of biogenesis and quality-control factors cooperate to ensure the assembly of the catalytic mitoribosome.

RESOURCE AVAILABILITY

Lead contact

Further information and requests for resources should be directed to and will be fulfilled by the lead contact, Alexey Amunts (alexey.amunts@gmail.com).

Materials availability

This study did not generate any new unique materials.

Data and code availability

- The atomic model of the *T. brucei* mtSSU precursor was deposited in the PDB database (PDB ID 9HNY) and is publicly available as of the date of publication. All data from phylogenetic and structural analyses are available as Supplemental Information or have been deposited on Figshare (<https://doi.org/10.6084/m9.figshare.29254817>) and are publicly available as of the date of publication.
- This paper does not report original code.
- Any additional information required to reanalyze the data reported in this paper is available from the lead contact upon request.

ACKNOWLEDGMENTS

This work was supported by the European Research Council (ERC-2018-StG-805230) to A.A., Czech Science Foundation (20-04150Y) and the Ministry of Education, Youth and Sports of the Czech Republic through the e-INFRA CZ (ID:90254) to O.G., Horizon Europe ERC MitoSignal project no. 101044951 to A.Z., the project P JAC CZ.02.01.01/00/22_008/0004575 RNA for therapy, co-funded by the European Union to A.Z. and O.G., and SciLifeLab Beyond-Fold to B.N. G.W. and P.C.W. were supported by NIH grant R35GM153502-01. Some of the structure prediction experiments and other analyses were enabled by the Berzelius resource provided by the Knut and Alice Wallenberg Foundation at the National Supercomputer Center in Sweden. Work in the Center for Theoretical Biological Physics was supported by the National Science Foundation grant PHY-2210291. We thank members of Amunts lab for their contributions to model building, data interpretation, and discussions.

AUTHOR CONTRIBUTIONS

Y.Z. built the model; C.M. carried out computational modeling and structure prediction; G.W. and P.C.W. performed molecular simulations; Y.Z., C.M., G.W., P.C., P.C.W., O.G., and A.A. performed the structural analysis; T.P. performed the phylogenetic analysis; B.N. and A.Z. supervised the project; A.A. and O.G. wrote the manuscript with help from Y.Z. and P.C.W. All the authors contributed to the manuscript preparation.

DECLARATION OF INTERESTS

The authors declare no competing interests.

STAR★METHODS

Detailed methods are provided in the online version of this paper and include the following:

- KEY RESOURCES TABLE
- METHOD DETAILS
 - Model building
 - Structure prediction and analyses
 - Identification and phylogenetic analyses of Mettl15 and Mettl17 across eukaryotes
 - Molecular dynamics simulations
- QUANTIFICATION AND STATISTICAL ANALYSIS

SUPPLEMENTAL INFORMATION

Supplemental information can be found online at <https://doi.org/10.1016/j.str.2025.08.002>.

Received: February 3, 2025

Revised: May 21, 2025

Accepted: August 4, 2025

REFERENCES

- Singh, V., Moran, J.C., Itoh, Y., Soto, I.C., Fontanesi, F., Couvillion, M., Huynen, M.A., Churchman, L.S., Barrientos, A., and Amunts, A. (2024). Structural basis of LRPPRC-SLIRP-dependent translation by the mitoribosome. *Nat. Struct. Mol. Biol.* *31*, 1838–1847. <https://doi.org/10.1038/s41594-024-01365-9>.
- Itoh, Y., Andréll, J., Choi, A., Richter, U., Maiti, P., Best, R.B., Barrientos, A., Battersby, B.J., and Amunts, A. (2021). Mechanism of membrane-tethered mitochondrial protein synthesis. *Science* *371*, 846–849. <https://doi.org/10.1126/science.abe0763>.
- Ott, M., Amunts, A., and Brown, A. (2016). Organization and Regulation of Mitochondrial Protein Synthesis. *Annu. Rev. Biochem.* *85*, 77–101. <https://doi.org/10.1146/annurev-biochem-060815-014334>.
- Singh, V., Itoh, Y., Del'Olivo, S., Hassan, A., Naschberger, A., Flygaard, R. K., Nobe, Y., Izumikawa, K., Aibara, S., Andréll, J., et al. (2024). Mitoribosome structure with cofactors and modifications reveals mechanism of ligand binding and interactions with L1 stalk. *Nat. Commun.* *15*, 4272. <https://doi.org/10.1038/s41467-024-48163-x>.
- Amunts, A., Brown, A., Toots, J., Scheres, S.H.W., and Ramakrishnan, V. (2015). Ribosome. The structure of the human mitochondrial ribosome. *Science* *348*, 95–98. <https://doi.org/10.1126/science.aaa1193>.
- Greber, B.J., Bieri, P., Leibundgut, M., Leitner, A., Aebersold, R., Boehringer, D., and Ban, N. (2015). Ribosome. The complete structure of the 55S mammalian mitochondrial ribosome. *Science* *348*, 303–308. <https://doi.org/10.1126/science.aaa3872>.
- Lavdovskaia, E., Hanitsch, E., Linden, A., Pašen, M., Challa, V., Horokhovskiy, Y., Roetschke, H.P., Nadler, F., Welp, L., Steube, E., et al. (2024). A roadmap for ribosome assembly in human mitochondria. *Nat. Struct. Mol. Biol.* *31*, 1898–1908. <https://doi.org/10.1038/s41594-024-01356-w>.
- Brischigliaro, M., Sierra-Magro, A., Ahn, A., and Barrientos, A. (2024). Mitochondrial ribosome biogenesis and redox sensing. *FEBS Open Bio* *14*, 1640–1655. <https://doi.org/10.1002/2211-5463.13844>.
- Conor Moran, J., Del'Olivo, S., Choi, A., Zhong, H., and Barrientos, A. (2023). Mitoribosome Biogenesis. *Methods Mol. Biol.* *2667*, 23–51. https://doi.org/10.1007/978-1-0716-3171-3_3.
- Khawaja, A., Cipullo, M., Kruger, A., and Rorbach, J. (2023). Insights into mitoribosomal biogenesis from recent structural studies. *Trends Biochem. Sci.* *48*, 629–641. <https://doi.org/10.1016/j.tibs.2023.04.002>.
- Haas, R.H. (2019). Mitochondrial Dysfunction in Aging and Diseases of Aging. *Biology* *8*, 48. <https://doi.org/10.3390/biology8020048>.
- Hong, H.J., Joung, K.H., Kim, Y.K., Choi, M.J., Kang, S.G., Kim, J.T., Kang, Y.E., Chang, J.Y., Moon, J.H., Jun, S., et al. (2022). Mitoribosome insufficiency in beta cells is associated with type 2 diabetes-like islet failure. *Exp. Mol. Med.* *54*, 932–945. <https://doi.org/10.1038/s12276-022-00797-x>.
- Richman, T.R., Ermer, J.A., Siira, S.J., Kuznetsova, I., Brosnan, C.A., Rossetti, G., Baker, J., Perks, K.L., Cserne Szappanos, H., Viola, H.M., et al. (2021). Mitochondrial mistranslation modulated by metabolic stress causes cardiovascular disease and reduced lifespan. *Aging Cell* *20*, e13408. <https://doi.org/10.1111/acer.13408>.
- Pecina, P., Čunátová, K., Kaplanová, V., Puertas-Frías, G., Šilhavý, J., Tauchmannová, K., Vrbáček, M., Čajka, T., Gahura, O., Hlaváčková, M., et al. (2024). Haplotype variability in mitochondrial rRNA predisposes to metabolic syndrome. *Commun. Biol.* *7*, 1116. <https://doi.org/10.1038/s42003-024-06819-w>.
- Saurer, M., Ramrath, D.J.F., Niemann, M., Calderaro, S., Prange, C., Mattei, S., Scaiola, A., Leitner, A., Bieri, P., Horn, E.K., et al. (2019). Mitoribosomal small subunit biogenesis in trypanosomes involves an extensive assembly machinery. *Science* *365*, 1144–1149. <https://doi.org/10.1126/science.aaw5570>.
- Soufari, H., Waltz, F., Parrot, C., Durrieu-Gaillard, S., Boehler, A., Kuhn, L., Sissler, M., and Hashem, Y. (2020). Structure of the mature kinetoplastids mitoribosome and insights into its large subunit biogenesis. *Proc. Natl. Acad. Sci. USA* *117*, 29851–29861. <https://doi.org/10.1073/pnas.2011301117>.
- Jaskolowski, M., Ramrath, D.J.F., Bieri, P., Niemann, M., Mattei, S., Calderaro, S., Leibundgut, M., Horn, E.K., Boehringer, D., Schneider, A., and Ban, N. (2020). Structural Insights into the Mechanism of Mitoribosomal Large Subunit Biogenesis. *Mol. Cell* *79*, 629–644.e4. <https://doi.org/10.1016/j.molcel.2020.06.030>.
- Tobiasson, V., Gahura, O., Aibara, S., Baradaran, R., Ziková, A., and Amunts, A. (2021). Interconnected assembly factors regulate the biogenesis of mitoribosomal large subunit. *EMBO J.* *40*, e106292. <https://doi.org/10.15252/embj.2020106292>.
- Lenarcic, T., Niemann, M., Ramrath, D.J.F., Calderaro, S., Flugel, T., Saurer, M., Leibundgut, M., Boehringer, D., Prange, C., Horn, E.K., et al. (2022). Mitoribosomal small subunit maturation involves formation of initiation-like complexes. *Proc. Natl. Acad. Sci. USA* *119*, e2114710118. <https://doi.org/10.1073/pnas.2114710118>.
- Kummer, E., Leibundgut, M., Rackham, O., Lee, R.G., Boehringer, D., Filipovska, A., and Ban, N. (2018). Unique features of mammalian mitochondrial translation initiation revealed by cryo-EM. *Nature* *560*, 263–267. <https://doi.org/10.1038/s41586-018-0373-y>.
- Khawaja, A., Itoh, Y., Remes, C., Spåhr, H., Yukhnovets, O., Höfig, H., Amunts, A., and Rorbach, J. (2020). Distinct pre-initiation steps in human mitochondrial translation. *Nat. Commun.* *11*, 2932. <https://doi.org/10.1038/s41467-020-16503-2>.
- Itoh, Y., Khawaja, A., Laptev, I., Cipullo, M., Atanassov, I., Sergiev, P., Rorbach, J., and Amunts, A. (2022). Mechanism of mitoribosomal small subunit biogenesis and preinitiation. *Nature* *606*, 603–608. <https://doi.org/10.1038/s41586-022-04795-x>.
- Itoh, Y., Singh, V., Khawaja, A., Naschberger, A., Nguyen, M.D., Rorbach, J., and Amunts, A. (2022). Structure of the mitoribosomal small subunit with streptomycin reveals Fe-S clusters and physiological molecules. *eLife* *11*, e77460. <https://doi.org/10.7554/eLife.77460>.
- Aibara, S., Singh, V., Modelska, A., and Amunts, A. (2020). Structural basis of mitochondrial translation. *eLife* *9*, e58362. <https://doi.org/10.7554/eLife.58362>.
- Pham, T.C.P., Raun, S.H., Havula, E., Henriquez-Olguin, C., Rubalcava-Gracia, D., Frank, E., Fritzen, A.M., Jannig, P.R., Andersen, N.R., Kruse, R., et al. (2024). The mitochondrial mRNA-stabilizing protein SLIRP regulates skeletal muscle mitochondrial structure and respiration by exercise-recoverable mechanisms. *Nat. Commun.* *15*, 9826. <https://doi.org/10.1038/s41467-024-54183-4>.
- Harper, N.J., Burnside, C., and Klinge, S. (2023). Principles of mitoribosomal small subunit assembly in eukaryotes. *Nature* *614*, 175–181. <https://doi.org/10.1038/s41586-022-05621-0>.
- Ast, T., Itoh, Y., Sadre, S., McCoy, J.G., Namkoong, G., Wengrod, J.C., Chicherin, I., Joshi, P.R., Kamenski, P., Suess, D.L.M., et al. (2024). METTL17 is an Fe-S cluster checkpoint for mitochondrial translation. *Mol. Cell* *84*, 359–374.e8. <https://doi.org/10.1016/j.molcel.2023.12.016>.
- Evans, R., O'Neill, M., Pritzel, A., Antropova, N., Senior, A., Green, T., Židek, A., Bates, R., Blackwell, S., Yim, J., et al. (2022). Protein complex prediction with AlphaFold-Multimer. Preprint at bioRxiv. <https://doi.org/10.1101/2021.10.04.463034>.
- Wallner, B., Amunts, A., Naschberger, A., Nystedt, B., and Mirabello, C. (2022). dgram2dmap: Extraction, visualisation and formatting of distance

- constraints from AlphaFold distograms. Preprint at bioRxiv. <https://doi.org/10.1101/2022.12.08.519560>.
30. Jumper, J., and Hassabis, D. (2022). Protein structure predictions to atomic accuracy with AlphaFold. *Nat. Methods* 19, 11–12. <https://doi.org/10.1038/s41592-021-01362-6>.
31. Pu, Y.G., Jiang, Y.L., Ye, X.D., Ma, X.X., Guo, P.C., Lian, F.M., Teng, Y.B., Chen, Y., and Zhou, C.Z. (2011). Crystal structures and putative interface of *Saccharomyces cerevisiae* mitochondrial matrix proteins Mmf1 and Mam33. *J. Struct. Biol.* 175, 469–474. <https://doi.org/10.1016/j.jsb.2011.05.005>.
32. Jiang, J., Zhang, Y., Krainer, A.R., and Xu, R.M. (1999). Crystal structure of human p32, a doughnut-shaped acidic mitochondrial matrix protein. *Proc. Natl. Acad. Sci. USA* 96, 3572–3577. <https://doi.org/10.1073/pnas.96.7.3572>.
33. Waltz, F., Salinas-Giegé, T., Englmeier, R., Meichel, H., Soufari, H., Kuhn, L., Pfeffer, S., Förster, F., Engel, B.D., Giegé, P., et al. (2021). How to build a ribosome from RNA fragments in *Chlamydomonas* mitochondria. *Nat. Commun.* 12, 7176. <https://doi.org/10.1038/s41467-021-27200-z>.
34. Schedlbauer, A., Iturrioz, I., Ochoa-Lizarralde, B., Diercks, T., López-Alonso, J.P., Lavin, J.L., Kaminishi, T., Çapuni, R., Dhimole, N., de Astigarraga, E., et al. (2021). A conserved rRNA switch is central to decoding site maturation on the small ribosomal subunit. *Sci. Adv.* 7, eabf7547. <https://doi.org/10.1126/sciadv.abf7547>.
35. Bikmullin, A.G., Fatkhullin, B., Stetsenko, A., Gabdulkhakov, A., Garaeva, N., Nurullina, L., Klochkova, E., Golubev, A., Khusainov, I., Trachtman, N., et al. (2023). Yet Another Similarity between Mitochondrial and Bacterial Ribosomal Small Subunit Biogenesis Obtained by Structural Characterization of RbfA from *S. aureus*. *Int. J. Mol. Sci.* 24, 2118. <https://doi.org/10.3390/ijms24032118>.
36. Datta, P.P., Wilson, D.N., Kawazoe, M., Swami, N.K., Kaminishi, T., Sharma, M.R., Booth, T.M., Takemoto, C., Fucini, P., Yokoyama, S., and Agrawal, R.K. (2007). Structural aspects of RbfA action during small ribosomal subunit assembly. *Mol. Cell* 28, 434–445. <https://doi.org/10.1016/j.molcel.2007.08.026>.
37. Rozanska, A., Richter-Dennerlein, R., Rorbach, J., Gao, F., Lewis, R.J., Chrzanowska-Lightowlers, Z.M., and Lightowlers, R.N. (2017). The human RNA-binding protein RBFA promotes the maturation of the mitochondrial ribosome. *Biochem. J.* 474, 2145–2158. <https://doi.org/10.1042/BCJ20170256>.
38. Van Haute, L., Hendrick, A.G., D'Souza, A.R., Powell, C.A., Rebelo-Guiomar, P., Harbour, M.E., Ding, S., Fearnley, I.M., Andrews, B., and Minczuk, M. (2019). METTL15 introduces N4-methylcytidine into human mitochondrial 12S rRNA and is required for mitoribosome biogenesis. *Nucleic Acids Res.* 47, 10267–10281. <https://doi.org/10.1093/nar/gkz735>.
39. Laptév, I., Shvetsova, E., Levitskii, S., Serebryakova, M., Rubtsova, M., Zgodá, V., Bogdanov, A., Kamenski, P., Sergiev, P., and Dontsova, O. (2020). METTL15 interacts with the assembly intermediate of murine mitochondrial small ribosomal subunit to form m4C840 12S rRNA residue. *Nucleic Acids Res.* 48, 8022–8034. <https://doi.org/10.1093/nar/gkaa522>.
40. Mutti, C.D., Van Haute, L., and Minczuk, M. (2024). The catalytic activity of methyltransferase METTL15 is dispensable for its role in mitochondrial ribosome biogenesis. *RNA Biol.* 21, 23–30. <https://doi.org/10.1080/15476286.2024.2369374>.
41. Chen, H., Shi, Z., Guo, J., Chang, K.J., Chen, Q., Yao, C.H., Haigis, M.C., and Shi, Y. (2020). The human mitochondrial 12S rRNA m(4)C methyltransferase METTL15 is required for mitochondrial function. *J. Biol. Chem.* 295, 8505–8513. <https://doi.org/10.1074/jbc.RA119.012127>.
42. Mashkovskaia, A.V., Mariasina, S.S., Serebryakova, M.V., Rubtsova, M. P., Dontsova, O.A., and Sergiev, P.V. (2023). Testing a Hypothesis of 12S rRNA Methylation by Putative METTL17 Methyltransferase. *Acta Naturae* 15, 75–82. <https://doi.org/10.32607/actanaturae.25441>.
43. Shi, Z., Xu, S., Xing, S., Yao, K., Zhang, L., Xue, L., Zhou, P., Wang, M., Yan, G., Yang, P., et al. (2019). Mettl17, a regulator of mitochondrial ribosomal RNA modifications, is required for the translation of mitochondrial coding genes. *FASEB J.* 33, 13040–13050. <https://doi.org/10.1096/fj.201901331R>.
44. Mirabello, C., Wallner, B., Nystedt, B., Azinas, S., and Carroni, M. (2024). Unmasking AlphaFold to integrate experiments and predictions in multimeric complexes. *Nat. Commun.* 15, 8724. <https://doi.org/10.1038/s41467-024-52951-w>.
45. Zhong, H., Janer, A., Khalimonchuk, O., Antonicka, H., Shoubridge, E.A., and Barrientos, A. (2023). BOLA3 and NFU1 link mitoribosome iron-sulfur cluster assembly to multiple mitochondrial dysfunctions syndrome. *Nucleic Acids Res.* 51, 11797–11812. <https://doi.org/10.1093/nar/gkad842>.
46. Gahura, O., Chauhan, P., and Ziková, A. (2022). Mechanisms and players of mitoribosomal biogenesis revealed in trypanosomatids. *Trends Parasitol.* 38, 1053–1067. <https://doi.org/10.1016/j.pt.2022.08.010>.
47. Burki, F., Roger, A.J., Brown, M.W., and Simpson, A.G.B. (2020). The New Tree of Eukaryotes. *Trends Ecol. Evol.* 35, 43–55. <https://doi.org/10.1016/j.tree.2019.08.008>.
48. Tyc, J., Novotna, L., Pena-Diaz, P., Maslov, D.A., and Lukes, J. (2017). RSM22, mtYsxC and PNKD-like proteins are required for mitochondrial translation in *Trypanosoma brucei*. *Mitochondrion* 34, 67–74. <https://doi.org/10.1016/j.mito.2017.01.003>.
49. Dimmer, K.S., Fritz, S., Fuchs, F., Messerschmitt, M., Weinbach, N., Neupert, W., and Westermann, B. (2002). Genetic basis of mitochondrial function and morphology in *Saccharomyces cerevisiae*. *Mol. Biol. Cell* 13, 847–853. <https://doi.org/10.1091/mbc.01-12-0588>.
50. Petrov, A.S., Wood, E.C., Bernier, C.R., Norris, A.M., Brown, A., and Amunts, A. (2019). Structural Patching Fosters Divergence of Mitochondrial Ribosomes. *Mol. Biol. Evol.* 36, 207–219. <https://doi.org/10.1093/molbev/msy221>.
51. Krissinel, E., and Henrick, K. (2007). Inference of macromolecular assemblies from crystalline state. *J. Mol. Biol.* 372, 774–797. <https://doi.org/10.1016/j.jmb.2007.05.022>.
52. Zhu, W., Shenoy, A., Kundrotas, P., and Elofsson, A. (2023). Evaluation of AlphaFold-Multimer prediction on multi-chain protein complexes. *Bioinformatics* 39, btad424. <https://doi.org/10.1093/bioinformatics/btad424>.
53. Case, D.A., Cheatham, T.E., 3rd, Darden, T., Gohlke, H., Luo, R., Merz, K. M., Jr., Onufriev, A., Simmerling, C., Wang, B., and Woods, R.J. (2005). The Amber biomolecular simulation programs. *J. Comput. Chem.* 26, 1668–1688. <https://doi.org/10.1002/jcc.20290>.
54. Noel, J.K., Levi, M., Raghunathan, M., Lammert, H., Hayes, R.L., Onuchic, J.N., and Whitford, P.C. (2016). SMOG 2: A Versatile Software Package for Generating Structure-Based Models. *PLoS Comput. Biol.* 12, e1004794. <https://doi.org/10.1371/journal.pcbi.1004794>.
55. Whitford, P.C., Geggier, P., Altman, R.B., Blanchard, S.C., Onuchic, J.N., and Sanbonmatsu, K.Y. (2010). Accommodation of aminoacyl-tRNA into the ribosome involves reversible excursions along multiple pathways. *RNA* 16, 1196–1204. <https://doi.org/10.1261/ma.2035410>.
56. Jackson, J., Nguyen, K., and Whitford, P.C. (2015). Exploring the balance between folding and functional dynamics in proteins and RNA. *Int. J. Mol. Sci.* 16, 6868–6889. <https://doi.org/10.3390/ijms16046868>.
57. Byju, S., Hassan, A., and Whitford, P.C. (2024). The energy landscape of the ribosome. *Biopolymers* 115, e23570. <https://doi.org/10.1002/bip.23570>.
58. Freitas, F.C., Fuchs, G., de Oliveira, R.J., and Whitford, P.C. (2021). The dynamics of subunit rotation in a eukaryotic ribosome. *Biophysica* 1, 204–221. <https://doi.org/10.3390/biophysica1020016>.
59. Whitford, P.C., Onuchic, J.N., and Sanbonmatsu, K.Y. (2010). Connecting energy landscapes with experimental rates for aminoacyl-tRNA accommodation in the ribosome. *J. Am. Chem. Soc.* 132, 13170–13171. <https://doi.org/10.1021/ja1061399>.
60. Heinrichs, M., Finke, A.F., Aibara, S., Krempler, A., Boshnakovska, A., Rehling, P., Hillen, H.S., and Richter-Dennerlein, R. (2025). Coupling of ribosome biogenesis and translation initiation in human mitochondria. *Nat. Commun.* 16, 3641. <https://doi.org/10.1038/s41467-025-58827-x>.

61. Glasgow, R.I.C., Singh, V., Peña-Pérez, L., Wilhalm, A., Moedas, M.F., Moore, D., Rosenberger, F.A., Li, X., Atanassov, I., Saba, M., et al. (2024). The mitochondrial methylation potential gates mitoribosome assembly. *Nat. Commun.* 16, 5388.
62. Averina, O.A., Laptév, I.G., Emelianova, M.A., Permyakov, O.A., Mariasina, S. S., Nikiforova, A.I., Mansikh, V.N., Grigorieva, O.O., Bolikhova, A.K., Kalabin, G.A., et al. (2022). Mitochondrial rRNA Methylation by Mett115 Contributes to the Exercise and Learning Capability in Mice. *Int. J. Mol. Sci.* 23, 6056. <https://doi.org/10.3390/ijms23116056>.
63. Li, H., Yu, K., Hu, H., Zhang, X., Zeng, S., Li, J., Dong, X., Deng, X., Zhang, J., and Zhang, Y. (2024). METTL17 coordinates ferroptosis and tumorigenesis by regulating mitochondrial translation in colorectal cancer. *Redox Biol.* 71, 103087. <https://doi.org/10.1016/j.redox.2024.103087>.
64. Su, B., Huang, K., Peng, Z., Amunts, A., and Yang, J. (2024). Improved automated model building for cryo-EM maps using CryFold. Preprint at bioRxiv. <https://doi.org/10.1101/2024.11.13.623164>.
65. Jamali, K., Käll, L., Zhang, R., Brown, A., Kimanius, D., and Scheres, S.H.W. (2024). Automated model building and protein identification in cryo-EM maps. *Nature* 628, 450–457. <https://doi.org/10.1038/s41586-024-07215-4>.
66. Wang, X., Zhu, H., Terashi, G., Taluja, M., and Kihara, D. (2024). DiffModeler: large macromolecular structure modeling for cryo-EM maps using a diffusion model. *Nat. Methods* 21, 2307–2317. <https://doi.org/10.1038/s41592-024-02479-0>.
67. Lewis, S., Hempel, T., Jiménez Luna, J., Gastegger, M., Xie, Y., Foong, A.Y. K., García Satorras, V., Abdin, O., Veeling, B.S., Zaporozhets, I., et al. (2024). Scalable emulation of protein equilibrium ensembles with generative deep learning. Preprint at bioRxiv. <https://doi.org/10.1101/2024.12.05.626885>.
68. Richter, D.J., Berney, C., Strassert, J.F.H., Poh, Y.-P., Herman, E.K., Muñoz-Gómez, S.A., Wideman, J.G., Burki, F., and de Vargas, C. (2022). EukProt: A database of genome-scale predicted proteins across the diversity of eukaryotes. *Peer Community J.* 2, e56. <https://doi.org/10.24072/pcjournal.173>.
69. Abramson, J., Adler, J., Dunger, J., Evans, R., Green, T., Pritzel, A., Ronneberger, O., Willmore, L., Ballard, A.J., Bambrick, J., et al. (2024). Accurate structure prediction of biomolecular interactions with AlphaFold 3. *Nature* 630, 493–500. <https://doi.org/10.1038/s41586-024-07487-w>.
70. Mistry, J., Finn, R.D., Eddy, S.R., Bateman, A., and Punta, M. (2013). Challenges in homology search: HMMER3 and convergent evolution of coiled-coil regions. *Nucleic Acids Res.* 41, e121. <https://doi.org/10.1093/nar/gkt263>.
71. Altschul, S.F., Madden, T.L., Schäffer, A.A., Zhang, J., Zhang, Z., Miller, W., and Lipman, D.J. (1997). Gapped BLAST and PSI-BLAST: a new generation of protein database search programs. *Nucleic Acids Res.* 25, 3389–3402. <https://doi.org/10.1093/nar/25.17.3389>.
72. Katoh, K., and Standley, D.M. (2013). MAFFT multiple sequence alignment software version 7: improvements in performance and usability. *Mol. Biol. Evol.* 30, 772–780. <https://doi.org/10.1093/molbev/mst010>.
73. Nguyen, L.T., Schmidt, H.A., von Haeseler, A., and Minh, B.Q. (2015). IQ-TREE: a fast and effective stochastic algorithm for estimating maximum-likelihood phylogenies. *Mol. Biol. Evol.* 32, 268–274. <https://doi.org/10.1093/molbev/msu300>.
74. de Oliveira, A.B., Jr., Contessoto, V.G., Hassan, A., Byju, S., Wang, A., Wang, Y., Doderro-Rojas, E., Mohanty, U., Noel, J.K., Onuchic, J.N., and Whitford, P. C. (2022). SMOG 2 and OpenSMOG: Extending the limits of structure-based models. *Protein Sci.* 31, 158–172. <https://doi.org/10.1002/pro.4209>.
75. Eastman, P., Galvelis, R., Peláez, R.P., Abreu, C.R.A., Farr, S.E., Gallicchio, E., Gorenko, A., Henry, M.M., Hu, F., Huang, J., et al. (2024). OpenMM 8: Molecular Dynamics Simulation with Machine Learning Potentials. *J. Phys. Chem. B* 128, 109–116. <https://doi.org/10.1021/acs.jpcc.3c06662>.
76. Meng, E.C., Goddard, T.D., Pettersen, E.F., Couch, G.S., Pearson, Z.J., Morris, J.H., and Ferrin, T.E. (2023). UCSF ChimeraX: Tools for structure building and analysis. *Protein Sci.* 32, e4792. <https://doi.org/10.1002/pro.4792>.
77. Afonine, P.V., Poon, B.K., Read, R.J., Sobolev, O.V., Terwilliger, T.C., Urzhumtsev, A., and Adams, P.D. (2018). Real-space refinement in PHENIX for cryo-EM and crystallography. *Acta Crystallogr. D Struct. Biol.* 74, 531–544.
78. Hassan, A., Byju, S., Freitas, F.C., Roc, C., Pender, N., Nguyen, K., Kimbrough, E.M., Mattingly, J.M., Gonzalez, R.L., Jr., de Oliveira, R.J., et al. (2023). Ratchet, swivel, tilt and roll: a complete description of subunit rotation in the ribosome. *Nucleic Acids Res.* 51, 919–934. <https://doi.org/10.1093/nar/gkac1211>.
79. Nguyen, K., and Whitford, P.C. (2016). Steric interactions lead to collective tilting motion in the ribosome during mRNA-tRNA translocation. *Nat. Commun.* 7, 10586. <https://doi.org/10.1038/ncomms10586>.
80. Whitford, P.C., Noel, J.K., Gosavi, S., Schug, A., Sanbonmatsu, K.Y., and Onuchic, J.N. (2009). An all-atom structure-based potential for proteins: Bridging minimal models with all-atom empirical forcefields. *Proteins: Structure, Function, Bioinformatics* 75, 430–441. <https://doi.org/10.1002/prot.22253>.

STAR★METHODS

KEY RESOURCES TABLE

REAGENT or RESOURCE	SOURCE	IDENTIFIER
Deposited data		
Atomic model of <i>T. brucei</i> pre-mtSSU	This study	PDB-9HNY
CryoEM map of <i>T. brucei</i> pre-mtSSU	Saurer et al. ¹⁵	EMDB-10180
Atomic model of mammalian pre-mtSSU	Itoh et al. ²²	PDB-7PNX
Atomic models of mammalian pre-mtSSU	Harper et al. ²⁶	PDB-8CSP, 8CST
Atomic model of <i>T. brucei</i> pre-mtSSU	Saurer et al. ¹⁵	PDB-6SGB
EukProt v3 Database	Richter et al. ⁶⁸	https://evocellbio.com/eukprot/
Phylogenetic and structural analyses	This study	https://doi.org/10.6084/m9.figshare.29254817
Software and Algorithms		
AlphaFold 3	Abramson et al. ^{30,69}	https://alphafoldserver.com/
AlphaFold Multimer	Evans et al. ²⁸	N/A
AF_unmasked	Mirabello et al. ⁴⁴	https://github.com/clami66/AF_unmasked
PyMOL	Schrödinger, Inc.	https://www.pymol.org/
HMMER3	Mistry et al. ⁷⁰	http://hmmer.org/
blast p	Altschul et al. ⁷¹	https://blast.ncbi.nlm.nih.gov/Blast.cgi?PAGE=Proteins
MAFFT v7.407	Katoh et al. ⁷²	https://mafft.cbrc.jp/
IQ-TREE multicore v2.2.0.3	Nguyen et al. ⁷³	http://www.iqtree.org/
SMOG2 package	Noel et al. ⁵⁴	https://smog-server.org
Open SMOG Library	de Oliveira et al. ⁷⁴	https://github.com/smog-server/OpenSMOG
Open MM Library	Eastman et al. ⁷⁵	https://github.com/openmm/openmm
PDBePISA	Krissinel et al. ⁵¹	https://www.ebi.ac.uk/pdbe/pisa/
UCSF ChimeraX	Meng et al. ⁷⁶	https://www.cgl.ucsf.edu/chimerax/
Phenix	Afonine et al. ⁷⁷	https://phenix-online.org/

METHOD DETAILS

Model building

The PDB ID 6SGB¹⁵ was used as a starting point and modified as follows. The assembly factor, mt-SAF38 (Tb927.5.1720), was assigned to an unknown chain in the original model based on the local density (cryo-EM density map EMD-10180) and the presence of the protein in previously isolated trypanosomal mitoribosomal complexes¹⁹ as revealed by mass spectrometry. Several regions were added or extended in different proteins. In the protein mS53 (chain DF), residues 63–84 were included. N-terminal regions were extended in the models of the proteins mt-SAF10 (chain FA) and mt-SAF11 (chain FB) protein. In the protein mt-SAF5 (chain F5), residues 560–596, previously categorized as an unknown chain, was now modeled. Several proteins have been identified as homologs of assembly factors from other organisms: mt-SAF1 has been assigned as Mettl17, mt-SAF14 as Mettl15, and mt-SAF18 as RbfA. Structural similarity revealed three components of the heterotrimeric assembly mt-SAF16, mt-SAF19, and mt-SAF25 are homologs of the homotrimer-forming human protein p32, yeast Mam33, or algal mS105.

The model of rRNA was modified as follows. The linker between nucleotides 560–620 (h44, h45) was adjusted. Some regions with insufficient resolution quality of density were removed, namely nucleotides 208–226, 254–260, 349–353, 385–389, 397–417, 431–440, 489–510, and 523–529. Nucleotides 67–73, 80–87, 171–172, 183–189, 273–285, 322–324, and 366–374 were shown as ribose-phosphate backbones.

Several ligands were included in the model. Consistent with previous observations,²³ we identified the density corresponding to GTP in the protein mS29 and PO₄³⁻ in the protein mt-SAF29. Ligand in Mettl17 and Mettl15, originally assigned as S-adenosylhomocysteine (SAH) molecules were substituted with S-adenosylmethionines (SAM), because there is no evidence suggesting that these proteins exist in the post-catalytic state, and the presence of SAM is more plausible in the context of our results. Furthermore, the Zn²⁺ ion present in Mettl17 was replaced with an Fe₄S₄ iron-sulfur cluster, consistently with the density, identity of

coordinating residues and recent identification of iron-sulfur cluster in yeast and mammalian homologs. Unidentified chain UD was replaced with acetyl Co-A. Final refinement was performed with Phenix.real_space_refine v1.13_2998.⁷⁷

Structure prediction and analyses

Structure prediction was performed by AlphaFold3⁶⁹ or AlphaFold Multimer.²⁸ The latter was used with databases BFD, Mgnify 2018_12, Uniref. 30 2021_03, Uniref. 90 2023_04 to predict structures and calculate ipTM scores for Mettl15 in dimer with all assembly factors present in early mtSSU intermediate. For *T. brucei* homology model, the clash at the interface between Mettl15 and Mettl17 was fixed by running a relaxation procedure with the Amber potential as done in AlphaFold, and the knot between Mettl15 and RNA was fixed by inpainting as described in AF_unmasked.⁴⁴ Here, the Mettl15-Mettl17 complex was used as a multimeric template and the clashing loop was deleted from the template so that it could be rebuilt by AlphaFold. Fifty predictions were generated this way, and the one closest to the initial template (RMSD: 0.2) where the clash would be fixed when including the RNA was selected. We neither show nor interpret regions with pLDDT scores below 65 in any of the models. Angles between Mettl15 in different models were calculated using the PyMOL (Schrödinger Inc., US) built-in script angle_between_domains.

Identification and phylogenetic analyses of Mettl15 and Mettl17 across eukaryotes

Using *Escherichia coli*, *Homo sapiens*, and *Trypanosoma brucei* orthologs of Mettl15 and Mettl17 as queries for blastp search against the EukProt v3 database,⁶⁸ we built starting datasets that were subsequently cleaned from apparent eukaryotic contaminations using phylogenetically aware approach (identification of possible contaminants by visual inspection of phylogenetic tree followed by manual check of their origin). Cleaned datasets were used to build profiles hmm in HMMER3.⁷⁰ Next, 131 organisms that cover known eukaryotic diversity and whose genome or transcriptome assemblies are of a good quality were selected for the final search. This search was performed in three steps: 1/HMMER3 search with profiles hmm; 2/blastp search⁷¹ using query sequence from a closely related species; 3/tblastn search in corresponding nucleotide assembly (to exclude possibility that ortholog is missing due to an inaccurate protein prediction). Names of selected organisms, accession numbers of used assemblies, and tools that were used for successful search are indicated in the Table S2. Multiple sequence alignments of the homologous amino acid sequences were built using MAFFT v7.407 with the L-INS-i algorithm⁷² and were manually trimmed to exclude unreliably aligned regions. The maximum likelihood tree was inferred with IQ-TREE multicore v2.2.0.3⁷³ using the LG4X substitution model. Statistical support was assessed with 100 IQ-TREE non-parametric bootstrap replicates. Sequences of both proteins from all organisms are available in Data S1 and S2.

Molecular dynamics simulations

Potential energy function

An all-atom structure-based “SMOG” model⁵⁴ of the mitoribosome small subunit was used to probe the scale of structural fluctuations around the post-catalytic state and determine whether thermal energy is sufficient for Mettl15-bound SAM to approach C1486, or whether Mettl15 is more likely to be associated with a larger-scale rearrangement that would require transient dissociation from the ribosome. The force field that was used is a single-basin model where the post-catalytic structure (PDB ID 7PNX) was defined as the global potential energy minimum. The specific variant of the force field is available through the smog-server force field repository (<https://smog-server.org>), with entry name AA_PTM_Hassan24.v2. The functional form of the potential energy is given as:

$$U = \sum_{\text{bonds}} \frac{\epsilon_r}{2} (r_i - r_{i,0})^2 + \sum_{\text{angles}} \frac{\epsilon_\theta}{2} (\theta_i - \theta_{i,0})^2 + \sum_{\text{impropers}} \frac{\epsilon_{\chi_{imp}}}{2} (\chi_i - \chi_{i,0})^2 + \sum_{\text{planars}} \epsilon_{\text{planar}} [1 - \cos(2\chi_i)] + \sum_{\text{backbone dihedrals}} \epsilon_{\text{bb}} F(\phi_i - \phi_{i,0}) \\ + \sum_{\text{sidechain dihedrals}} \epsilon_{\text{sc}} F(\phi_i - \phi_{i,0}) + \sum_{\text{contacts}} \epsilon_c \left[\left(\frac{\sigma_{ij}}{r_{ij}} \right)^{12} - 2 \left(\frac{\sigma_{ij}}{r_{ij}} \right)^6 \right] + \sum_{\text{non-contacts}} \epsilon_{\text{nc}} \left(\frac{\sigma_{\text{nc}}}{\sigma_{ij}} \right)^{12}$$

where

$$F(\phi) = [1 - \cos(\phi)] + \frac{1}{2} [1 - \cos(3\phi)]$$

r_0 and θ_0 parameters are given values found in the Amber ff03 force field.⁷⁸ Dihedral parameters χ_0 and $\{\phi_0\}$ are assigned the corresponding values found in the experimental model. Non-bonded contacts that are found in the experimental model, are identified according to the Shadow Contact Map algorithm, with a shadowing radius of 1 Å and a cutoff distance of 6 Å. The contacts are given an attractive 6–12 interaction that stabilizes the preassigned structure, with interatomic distance σ_{ij} that is found in the experimental structure, multiplied by 0.96 to avoid artificial expansion of the structure.⁷⁹ Atom pairs that are not in contact are assigned a repulsive potential to model excluded-volume steric interactions, where σ_{nc} is given the value 2.5 Å. Energy scale weights are defined as $\epsilon_r = 100 \frac{\epsilon}{\text{Å}^2}$, $\epsilon_\theta = 80 \frac{\epsilon}{\text{rad}^2}$, $\epsilon_{\chi_{imp}} = 10 \frac{\epsilon}{\text{rad}^2}$, $\epsilon_{\chi_{planar}} = 40 \frac{\epsilon}{\text{rad}^2}$, $\epsilon_{\text{nc}} = 0.1 \epsilon$, where ϵ is the reduced energy unit. The dihedral and contact energy weights are normalized as in Whitford et al., Proteins, 2009.⁸⁰

Since rRNA residues near the Mettl15 binding site are disordered (unresolved or high B-factors) in the pre-catalytic structure, these regions were modeled as disordered. For this, stabilizing contacts and dihedrals for the flexible rRNA region (i.e., residues U1477 to C1494 and A1555 to G1570), were removed.

Two sets of simulations were performed. In the first set of simulations, a harmonic restraint was introduced, which ensured that the distance between C1486 and SAM (sulfur atom) adopted short values. The harmonic restraint had a minimum at 5 Å and the spring constant was $150 \frac{\text{e}}{\text{nm}^2}$. These simulations were used to ask whether simple bending motions of Mettl15 are sufficient for SAM and C1486 to become proximal. In the second set of simulations, the restraint was not included. These unrestrained simulations were performed to determine the scale and direction of structural fluctuations that can arise from thermal energy.

Simulation details

All force field files were generated using SMOG2 software package.⁵⁴ Molecular dynamics simulations were performed using OpenMM⁷⁵ and OpenSMOG⁷⁴ libraries. The simulations were performed at a reduced temperature of $0.5 \frac{\text{e}}{\text{K}_B}$ that was maintained by using Langevin dynamics protocols.

Calculating rotation angles for Mettl15

Euler angles were used to describe rotation of Mettl15, relative to the mtSSU body.⁷⁸ Consistent with methods for describing rotation of the mtSSU,⁷⁸ we described a rotation angle γ , which is the sum of the ψ and ϕ angles in the Euler formulation (Figure S4). The polar angle θ (i.e., tilt angle) represents rotation that is orthogonal to the primary rotation. To calculate Euler angles, we first assigned a set of axes that remain fixed in the frame of reference of Mettl15. For convenience, we define the “Z” axis as the axis of rotation (Euler-Rodrigues axis) between the pre and post catalytic states. The following protocol was used to define the primary rotation axis:

- (1) Least squares alignment of the mtSSU (excluding Mettl15) of the pre-catalytic structure to post-catalytic structure.
- (2) Associate coordinate system to Mettl15 of pre and post catalytic structures.
- (3) The E-R angle was then calculated between the coordinate systems of both structures. The angle was found to be 45°.

To calculate Euler angles in the simulations, the following protocol was applied.

- (1) Define “Z” axis as the E-R axis. This ensures that our primary rotation angle γ describes rotation that is parallel to that defined by the pre-to-post rearrangement.
- (2) Align each simulated frame to the post-catalytic structure of the mtSSU, where alignment was based on non-Mettl15 atoms.
- (3) Align the post-catalytic conformation of Mettl15 to each simulated frame.
- (4) Calculate the Euler angles (ϕ , ψ and θ) between the post-catalytic and aligned (previous step) orientation.
- (5) Define rotation as $\gamma = \phi + \psi$.
- (6) Define tilt as θ .

QUANTIFICATION AND STATISTICAL ANALYSIS

Refinement statistics are summarized in Table S3.